

Step Bunching: Influence of Impurities and Solution Flow

A.A. Chernov*, P.G. Vekilov**, S.R. Coriell***, B.T. Murray***, G.B. McFadden***

* Universities Space Research Association/MSFC, 4950 Corporate Drive,
Ste. 100, Huntsville, AL 35805

** University of Alabama in Huntsville, Huntsville, AL

***National Institute of Standards and Technology, Gaithersburg, MD 20899/999037090

S20-34

1. The Problem

Step bunching results in striations even at relatively early stages of its development and in inclusions of mother liquor at the later stages. Therefore, eliminating step bunching is crucial for high crystal perfection. At least 5 major effects causing and influencing step bunching are known:

1. Basic morphological instability of stepped interfaces. It is caused by concentration gradient in the solution normal to the face and by the redistribution of solute tangentially to the interface which redistribution enhances occasional perturbations in step density due to various types of noise.
2. Aggravation of the above basic instability by solution flowing tangentially to the face in the same directions as the steps or stabilization of equidistant step train if these flows are antiparallel [1-4].
3. Enhanced bunching at supersaturation where step velocity v increases with relative supersaturation s much faster than linear [5]. This $v(s)$ dependence is believed to be associated with impurities. The impurities of which adsorption time is comparable with the time needed to deposit one lattice layer may also be responsible for bunching [6, 7].
4. Very intensive solution flow stabilizes growing interface even at parallel solution and step flows [5].
5. Macrosteps were observed to nucleate at crystal corners and edges [8, 9]. Numerical simulation, assuming step-step interactions via surface diffusion also show that step bunching may be induced by random step nucleation at the facet edge and by discontinuity in the step density (a ridge) somewhere in the middle of a face. The corresponding bunching patterns produce the ones observed in experiment [10-12].

The nature of step bunching generated at the corners and edges and by dislocation step sources, as well as the also relative importance and interrelations between mechanisms 1-5 is not clear, both from experimental and theoretical standpoints. Furthermore, several laws controlling the evolution of existing step bunches have been suggested [13, 14], though unambiguous conclusions are still missing. Addressing these issues is the major goal of the present Project.

2. Theory [15]

Linear perturbation analysis was applied to a stepped interface on which step density is, respectively linear and non-linear functions of supersaturation and also to the case when the step rate is a non-linear function of supersaturation. The approach and codes developed earlier [1-4] were employed.

2.1 Linear increase of vicinal slope with supersaturation.

First vicinal slope, p , is kept constant. This is the case of, e.g., lysozyme faces or prismatic, KDP/ADP faces on which steps are generated by strong dislocation sources at high supersaturation. If $p = \text{const} = 5 \cdot 10^{-3}$ and the solution is stagnant, the interface is unstable within the area surrounded by solid line in Fig. 1. This solid line presents the perturbation wavevector k_x as a function of the normal growth rate, $V = pv$. As the solution flow velocity in the stabilizing (counter, or up-step) direction rises, this area of instability shrinks and disappears at a certain shear flow ($\sim < 1 \text{ s}^{-1}$ for the ADP growth parameters). The instability area expands if the flow is destabilizing (down-step).

If the vicinal slope p linearly increases with relative supersaturation ($p=0.117s$), the interface is stable in the area inside the dashed line in Fig. 1. In this case the instability region expands at higher growth rate rather than shrink, contrary to the region surrounded by the solid line and corresponding to $p = \text{const}$. Such dramatic change in behavior comes from much stronger sensitivity of the surface self stabilization to the average step density than to step velocity inducing the self stabilization.

2.2 Non-linear increase of step velocity and hillock slope with supersaturation.

Step velocity was chosen to fit the experimental data for prismatic ADP face making use of the following relationship

$$v = \beta_2 \{ b_1 + (b_2 - b_1) / [1 + \exp [b_3(1 - s/s^*)]] \} s \quad (1)$$

with $b_1 = 4.0 \cdot 10^{-3} \text{ cm/s}$, $b_2 = 3 \cdot 10^{-2} \text{ cm/s}$, $b_3 = 20$, $s^* = 0.041$. The square brackets present the stepwise function of s with the change from $\beta_2 \cong b_1$ at $s \ll s^*$ to $\beta_2 \cong b_2$ at $s \gg s^*$.

The resulting stability areas at different shear flows are seen in Fig. 2. The slope varied with supersaturation as $p = 0.117 \cdot s$. Besides the instability area in the upper right part of Fig. 2, similar to the one shown in Fig. 1, the instability also occurs at supersaturations $s \geq s^*$ where the kinetic coefficient changes most steeply with s . This confirms the experimentally observed and intuitively clear weaker stability of the interface to perturbations at the supersaturations corresponding to the strongest response of the interface to the local supersaturation changes i.e. impurity induced instability [5].

As it can be seen from Fig. 2 by comparing stability borders at various solution flow shear rates, S , the stability strongly depends on solution flow: the instability region in the middle of Fig. 2 may shrink to zero at high stabilizing shear flows, $S > 0$, and expands at $S < 0$. Experimentally, the impurity induced instability actually remains at any flow rates while theory predicts its elimination at sufficiently intense stirring. However, no systematic measurements at various flow rates have been performed so far.

If we assume that the hillock slope approaches constant value at rising supersaturations as it happens for powerful dislocation step sources, then the region in the upper right corner of Fig. 2 naturally disappears.

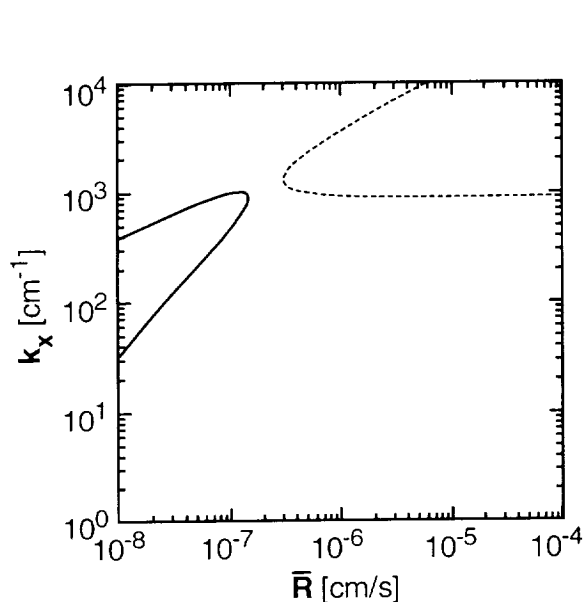


Fig. 1. The spatial wave numbers at which the system is neutrally stable as a function of growth velocity for linear kinetics ($b_0 = 0$, $b_1 = b_2 = 4.0 \times 10^{-3}$ cm/s) for $p = 0.005$ (solid curve) and $p = 0.117$ s (dashed curve).

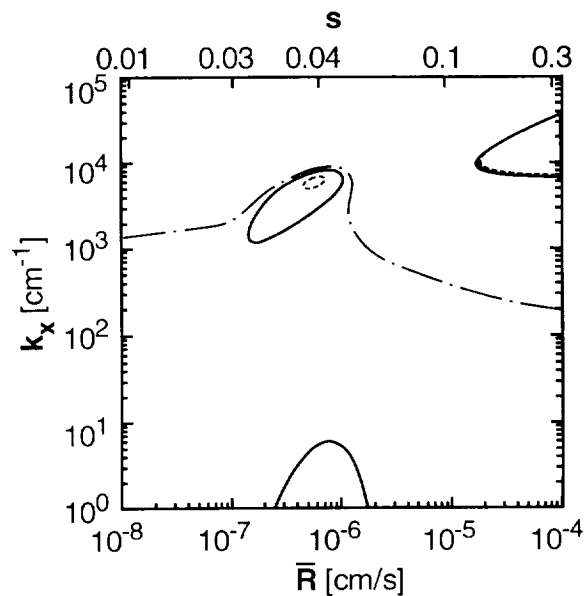


Fig. 2. The spatial wave numbers at which the system is neutrally stable as a function of growth velocity and supersaturation (upper axis) for nonlinear kinetics ($b_0 = 0$, $b_1 = 4.0 \times 10^{-3}$ cm/s, $b_2 = 3.0 \times 10^{-2}$ cm/s, $b_3 = 20.0$, $s^* = 0.041$) for $p = 0.117$ s and shear rates S of 0.5 (dashed), 0 (solid), and -0.5 (chain dashed) s^{-1} .

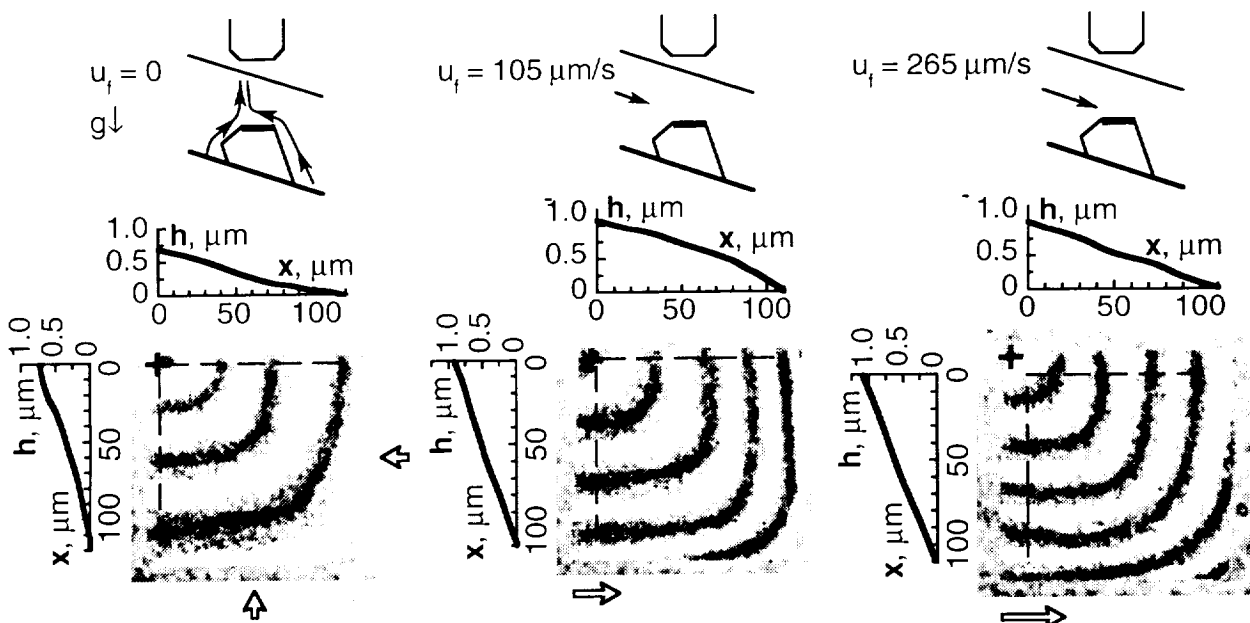


Fig. 3. Schematic of the experiment (upper row) of lysozyme crystal growing under conditions of natural convection (a), and forced flow at the average flow rates $u = 105 \mu\text{m/s}$ (b) and $265 \mu\text{m/s}$ (c). The face profiles shown at the interferograms were determined by interference pattern intensity along the vertical and horizontal dashed lines.

3. Experiment

3.1 The average surface profile.

So far, stability of lysozyme bipyramidal face was studied. The experimental setup was described earlier [11]. The observation scheme and flows are shown in Fig. 3, upper row. The face profile was determined from interferograms. The local face growth rate and local vicinal slope, i.e. the step density, were measured in points #1, 2, 3 marked by crosses on each of the face interferograms (Fig. 3, lower row). Point #1 is in the upper left corner, point #2 is the upper right, and point #3 is the lower left. In each point, the interface positions by two adjacent laser beams, ca. $3\mu\text{m}$ apart was simultaneously measured. Each testing point includes such pair of laser beams with the pair oriented normal to the average step direction (interference fringes). Techniques for measurement and evaluation of these fluctuations were described in ref. [11]. As the interferograms demonstrate. The step source was located in the upper left corner of the face. This source is probably of dislocation origin because there was no growth cessation at supersaturation $s \simeq 0.4$. In the experiments under consideration, $s \simeq 1$.

The surface profiles $h(x)$ along the dashed lines in horizontal and vertical cross sections are attached to the corresponding interferograms. The profiles in the direction normal to the flow (between the points #1 and #3) shown at the left from each interferogram in Fig. 3. These profiles are about flat, in Figs. 3b and c, while in Fig. 3b this profile is concave.

The profiles along the flow behave differently. Under conditions of only natural convection, Fig. 3a, the $h(x)$ profile shows that the face is slightly concave in the region $30 < x < 80\mu\text{m/s}$.

At the forced flow rate $u=105\mu\text{m/s}$ (Fig. 3b) the face is convex. The profile convexity disappears if the crystal is turned by some 20° or more around the axis normal to the face and solution flow. Such a turn means changes in flow patterns and, also, that mutual azimuthal orientation of the flow and step directions changes significantly.

At flow rate, $u=265\mu\text{m/s}$ the hillock slope is about constant. The face flatness may be attributed to a deeper kinetic control of the growth and thus essentially more constant supersaturation along the face.

3.2 Fine Structure of the Surface: Fluctuations.

Figs. 4, 5 and 6 corresponding to the Fig. 3a, b, and c, present the temporal fluctuations of normal growth rate and local slopes in testing points #1, #2 and #3.

These temporal fluctuations are the result of step bunches passing through the testing points, possessing different slopes, p , and thus providing different local normal growth rates, $V = pv$.

No essential difference can be seen between fluctuations in a and c of Figs. 5, and 6. This might be expected since the flow in all cases is essentially parallel to the steps in testing points #1(a) and #3(c) and thus should not strongly influence step bunching. A larger amplitudes of normal growth rate fluctuations can be noted in test point #2 as compared to #1 under conditions of natural convection (Fig. 4). In this case, indeed, the flow is stabilizing in #2 and destabilizing in #1. This effect was reported earlier in [1, 5, 12].

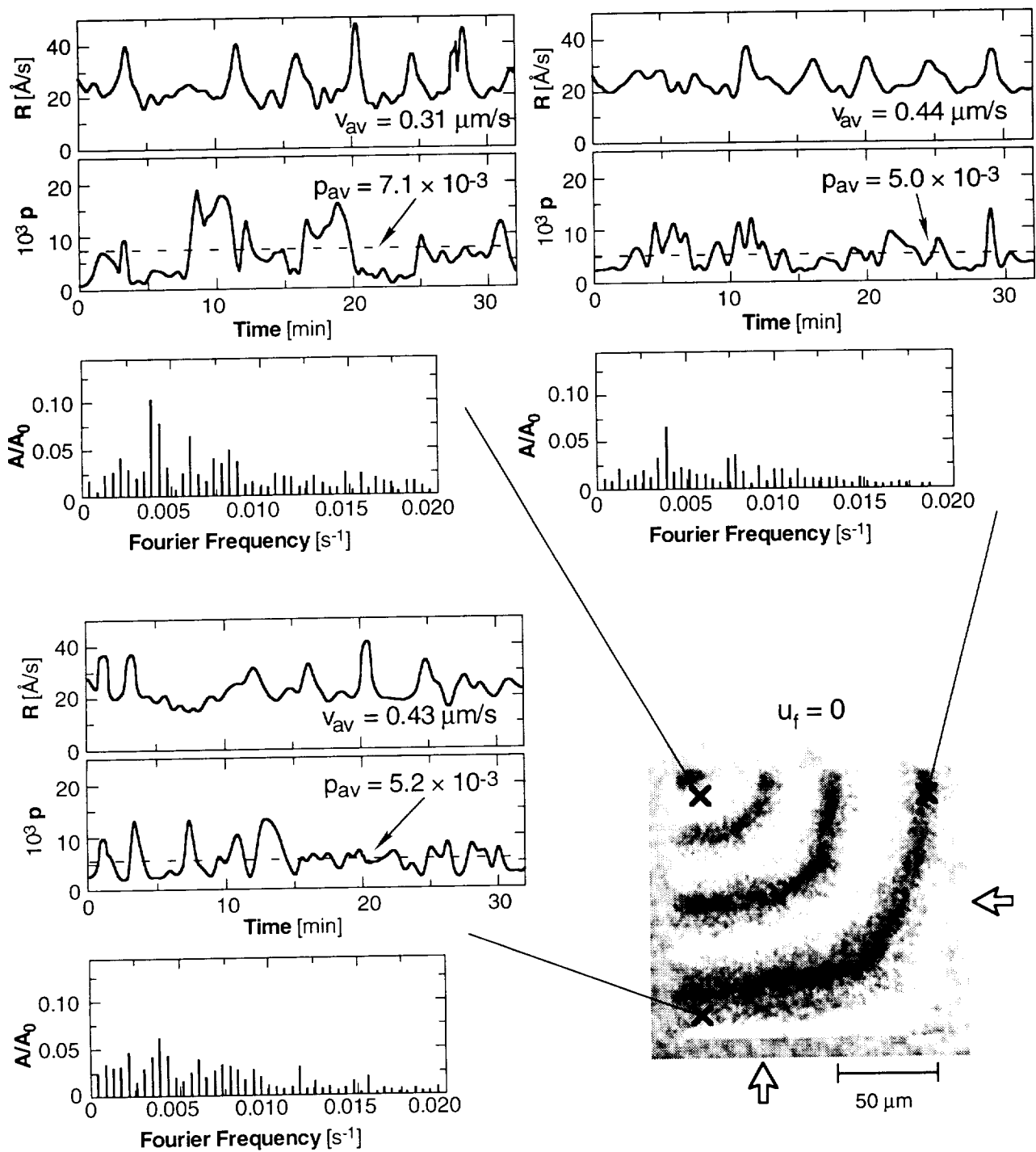


Fig. 4. Fluctuations in time, t , of the normal growth rate, $R(t)$, vicinal slope, $p(t)$ and Fourier Spectra of $R(t)$, shown as A/A_0 . Here A is the Fourier amplitude of the frequency plotted on abscissa, to the average growth rate $A_0=R_{av}(t)$. Data on a, b, c were measured at the points #1, #2, #3 shown in the interferogram d by crosses. Natural convective flow. Average slopes, p_{av} and effective step rates, v_{av} , are shown.

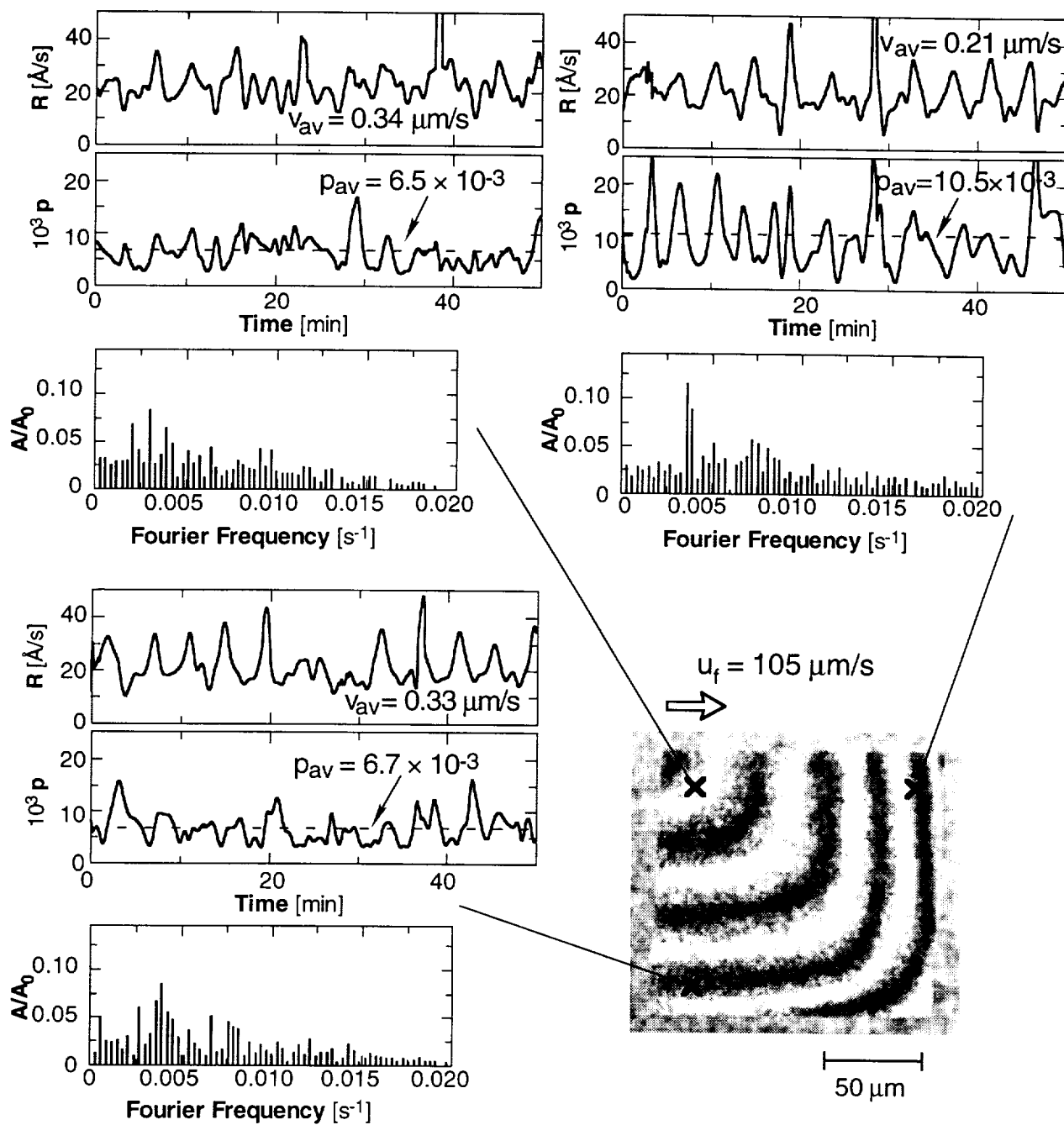


Fig. 5. Same as Fig. 4, forced solution flow rate $u = 105 \mu\text{m/s}$.

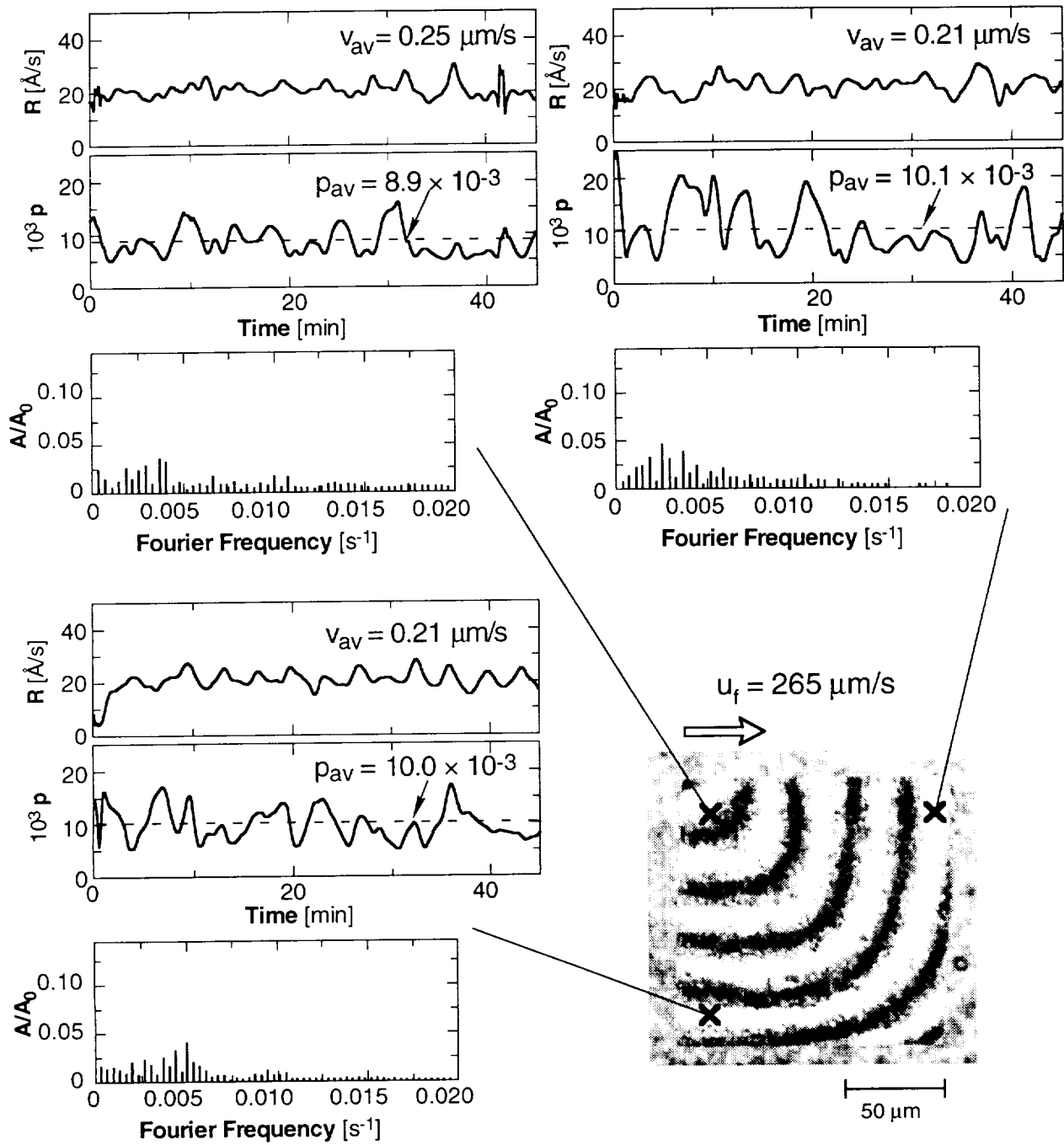


Fig. 6. Same as Fig. 4, forced solution flow rate $u = 265 \mu\text{m/s}$.

Comparing the fluctuation amplitude, in a and b in Figs. 5 and 6, we note that fluctuations are stronger in Figs. 5b, 6b as compared to Figs. 5a, 6a. This corresponds to an increase in average slope, p_{av} , from a to b. Similarly, the fluctuations are stronger in Fig. 4b at larger $p_{av}=7 \cdot 10^{-3}$ as compared to Fig. 4a at resulting $p_{av}=5 \cdot 10^{-3}$. Corresponding decrease in average step rate, v_a , with increase of p_{av} , may also be noted since the average normal growth rate, $R_{av} = (pv)_{av}$ remains unchanged. The numbers for p_{av} and v_{av} are given in the figures.

Much stronger effect have the increase in the flow rate from 105 $\mu\text{m/s}$ to 265 $\mu\text{m/s}$: fluctuations in normal growth rate in Fig. 5 are noticeably less intense than these in Fig. 6, i.e., the flow rate rise essentially damps the fluctuations. This effect takes place in both the upstream and the downstream testing points #1 and #2 in Figs. 6a and b. Simultaneously, an increase of the $p(t)$ and $R(t)$ fluctuations measured in the downstream points #2(b), as compared to the upstream point #1(a) can be seen in Fig. 5.

4. Discussion and Conclusions

The role of bulk transport in formation of the overall face profile, i.e. the $h(x)$ and $p(x)$ dependencies (Fig. 4), can be estimated making use of convectional boundary layer thickness above thin plate. With $R=2 \cdot 10^{-7} \text{cm/s}$, $D=10^{-6} \text{cm}^2/\text{s}$, $v=10^{-2} \text{g/cm.s}$, crystal size $\sim 100 \mu\text{m}$ and the ratio of the protein concentration in crystal to the one in solution $\simeq 30$, this estimate suggests the diffusion boundary layer thickness $\simeq 2.3 \cdot 10^{-2} \text{cm}$ and about 10% decrease in supersaturation along the face. This is insufficient to provide the observed slope change of the order of 100%.

This large slope increase may be associated with step bunching resulting in effectively lower average kinetic coefficient of the face. The corresponding modeling based on strong step-step interaction is consistent with this large increase — cf. Figs. 9 and 16 in ref. [10].

Existence of fluctuations corresponding to step bunches passing the test point #1, close to the step source, along with the ones in #2 and #3, suggests that the experimentally observed bunching might occur at the very beginning, during the step generation and is merely enhanced in course of propagation along the face. Therefore, the theory analyzing only onset of instability is probably insufficient to treat the data: evolution of bunches, along with their generation at the dislocation and/or nucleation sources is needed.

The mechanism of step bunching in the close proximity to the step source is not clear. One may think of step pairing noted on the KDP crystals by AFM [17], on bunching provided by irregular step generation at the edge with essential contribution of surface diffusion [12], on the coupled impurity adsorption, step nucleation and propagation [18] at supersaturations close to the transfer from the dislocation to the 2D nucleation driven growth and at the supersaturations close to the impurity assisted non-linear steep increase of the step rate with s , like the one discussed in Sec. 2.

Suppression of fluctuations by the faster solution flow may be associated with weaker coupling of step generation by either dislocations or 2D nucleation (both non-linearly dependent on supersaturation) with diffusion and impurity adsorption in the very vicinity of the step generation area.

Enhanced fluctuations in the downstream portion of the step train is qualitatively consistent with the theory developed in Sec. 2. However, extension of the theory to the evolution of the already formed surface corrugations to form the more pronounced dissipative step structure is needed. Equally important are relevant future experiments.

5. Acknowledgment

The Authors acknowledge the support of the NASA Microgravity Science and Applications Division through grants NAG8-1354 and NAG8-1454.

6. References

1. A.A. Chernov, Y.G. Kuznetsov, I.L. Smol'ski, V.N. Rozhanski, *Sov. Phys. Crystallography* **31** (1986) 859.
2. A.A. Chernov, *J. Cr. Gr.* **118** (1992) 705.
3. A.A. Chernov, S.R. Coriell, B.T. Murray, *J. Cr. Gr.* **132** (1993) 405.
4. S.R. Coriell, B.T. Murray, A.A. Chernov, G.B. McFadden, *J. Cr. Gr.* **169** (1996) 773, *Met. Matls Trans.* **27A** (1996) 687.
5. L.N. Rashkovich and B.Y. Shekunov, *J. Cr. Gr.* **100** (1990) 133.
6. F.C. Frank, in *Growth and Perfection of Crystals*, Ed. R.H. Doremus, B.W. Roberts, D. Turnbull (Chapman and Hill, London, 1958) p. **411**.
7. J. P. van der Eerden and H. Müller Krumbhaar *Electrochim. Acta* **31** (1986) 2431.
8. A. Papapetrou, *Zs. f. Kristallografie* **92** (1935) 89.
9. A.A. Chernov, *J. Cryst. Gr.* **24-25** (1974) 122.
10. P.G. Vekilov, H. Lin and F. Rosenberger, *Phys. Rev. E* **55** (1997) 3202.
11. P.G. Vekilov, L.A. Monaco and F. Rosenberger, *J. Cryst. Gr.* **146** (1995) 289.
12. P.G. Vekilov, J.I.D. Alexander and F. Rosenberger, *Phys. Rev.* **55** (1996) 6650.
13. A.A. Chernov, *Sov. Phys. Usp* **4** (1961) 116.
14. D.G. Vlachos, L.D. Schmidt, R. Aris, *Phys. Rev. B* **47** (1993) 4896.
15. S.R. Coriell, A.A. Chernov, B.T. Murray, G.B. McFadden, *J. Cryst. Gr.* **183** (1998) 669.
16. Carlson, ref. 6, p. **421**.
17. J.J. DeYoreo, T.A. Land, B. Daiz, *Phys. Rev. Lett.* **73** (1994) 838.
18. A.A. Chernov, V.F. Parvov, M.O. Kliya, D.V. Kostomarov, Y.G. Kuzentsov, *Sov. Phys. Crystal* **52** (1981) 185.

